Propane Dehydrogenation on Pt Single-atom and Pt_4 and Pt_3Sn Single-clusters Supported on g-C_3N_4. A Theoretical Study.

Jie Pan,[a] Evgenii Strugovschikov,[a] Antoni Salóm-Català,[a] Gerard Novell-Leruth,[b] Kamila Kaźmierczak,[c] Daniel Curulla-Ferré,[c] Jorge J. Carbó,[a] Cyril Godard,[a] and Josep M. Ricart,[a,]*

a) Departament de Química Física i Inorgànica, Universitat Rovira i Virgili, Tarragona, Spain.

b) Iberian Centre for Research in Energy Storage, Cáceres, Spain

c) TotalEnergies OneTech Belgium, Zone Industrielle Feluy C, Seneffe, Belgium

KEYWORDS: Density functional theory, DFT, Propane dehydrogenation, PDH, Single Atom Catalysis, SAC, Supported cluster, Platinum, Carbon nitride, Catalysis.

ABSTRACT

Propane dehydrogenation (PDH) is one of the most widely used processes to produce propylene. Platinum is an effective catalyst for PDH. However, metallic Pt facilitates deep dehydrogenation and coke formation. In contrast, small sub-nanoparticles and, at the limit, single atom catalysts (SACs) have shown high reactivity, prevent coke formation and are much cheaper. Graphitic carbon nitride (g-C_3N_4) has been used as a support for several catalytic and electrocatalytic

processes. In this work, three Pt-based catalysts, single-atom (Pt_1), single-cluster (Pt_4) and bimetallic Pt_3Sn anchored on the heptazine units of g-C_3N_4 were modelled using the density functional theory (DFT) approach in conjunction with microkinetic analysis. *Ab initio* molecular dynamics (AIMD) has been also used to assure the stability of the systems. All three systems showed good activity for PDH. However, we have shown that the conversion is only satisfactory at high temperatures, according to the thermodynamic and kinetic requirements, due to the high cost of propene desorption. On the other hand, the energy barriers for the deep dehydrogenation side reaction remain similar as the temperature increases. Substituting a Pt atom by Sn in Pt_4 to give a bimetallic subnanometric Pt_3Sn cluster, facilitates propene desorption and inhibits deep dehydrogenation and subsequent coke formation.

INTRODUCTION

Today, despite some unintended consequences, plastics have become an integral part of modern society, improving our quality of life. However, feedstocks such as propene are in short supply, and more than traditional light oil cracking methods is needed to meet demand.[1,2]

Instead, the conversion of propane, which is cheap and readily available, has attracted much attention. Oxidative and non-oxidative approaches convert propane to propene.[3] Oxidative dehydrogenation is an exothermic reaction that can achieve high conversion rates at low temperatures but can produce unwanted CO_x by-products due to the need for an oxidant (such as CO_2 and N_2O).[4,5] In contrast, non-oxidative propane dehydrogenation (PDH), is a more environmentally friendly process. However, direct PDH is endothermic, with $\Delta H° = 123.8$ kJ/mol at 298.15 K, only exergonic at high temperatures (~ 900 K), and only feasible using efficient catalysts.[6]

The most commonly used catalysts are those based on platinum, due to the high density of electronic states near the Fermi level, which exhibit good activity towards PDH because of their capability to activate C-H bonds.[7,8] Recently, molecular dynamic simulations using reactive force fields,[9] showed the following order of reactivity on platinum surfaces: Pt(111) < Pt(100) < Pt(211); and that propene activation on the most reactive one, stepped Pt(211) surface, occurs on low-coordinated Pt atoms at the steps. This is in line with the study by Terejanu, Heyden, *et al*.[10] combining DFT calculations with Bayesian statistics, which concluded that Pt(211) is the dominant active and selective facet of Pt catalysts. Thus, there is a clear correlation between the Pt surface and PDH activity. Using the activation energy difference between further dehydrogenation and propene desorption as a selectivity descriptor, Zhou *et al.*[11] reported that the selectivity towards propene is substantially lowered in the presence of the coordinately unsaturated surface Pt atoms. Therefore, there is no clear agreement on the effect of catalyst topology on selectivity. Undesired reactions in the PDH process involves deep dehydrogenations and C-C bond breaking and result in the formation of coke at the surface of the catalyst and deactivate it. To improve catalyst efficiency, the use of supported nanoparticles to inhibit deactivation was considered. As demonstrated by Sui, Chen, *et al.*[12] the dehydrogenation of propane over supported Pt particles is structurally sensitive. Reducing the Pt particle size to sub-nano clusters (<1 nm), particularly when atomically dispersed, significantly improved catalytic performance while maintaining high stability and selectivity for propene. In addition, Li, Su, *et al.*[13] studied the origin of coke formation using DFT based kinetic Monte Carlo simulations, and revealed that in the initial stages of PDH, a fast deactivation of the active sites at the metal surface takes place, where C_2/C_1 carbon species are tightly bonded. To improve the selectivity, bimetallic Pt-Sn systems were used, as Sn promotion is known to reduce the catalyst deactivation,[14] and can enhance the

dehydrogenation performance by shifting down the d-band center and thus reducing the adsorption energy of propene.[12,15] Therefore, the optimal scheme for designing catalysts for PDH would be highly dispersed nano or sub-nano metallic particles (monometallic and bimetallic), at the single atoms level on a suitable support such as oxides, carbon, or zeolites.[16]

The selection of suitable supports is a major challenge in the development of effective catalysts. Metal oxides and carbon-based materials are commonly used as supports due to their thermal stability and the abundance of metal-support interaction sites.[17,18,19,20,21,22,23] However, metal diffusion and surface aggregation are phenomena that can reduce catalyst efficiency.[6] To address this problem the use of supports with surfaces containing vacancies or holes that can capture metal atoms has been identified as an effective solution.[24,25,26] Graphitic carbon nitride (g-C_3N_4), also known as exfoliated carbon nitride (ECN), is a captivating non-metallic, non-toxic, low-cost and highly stable conjugated two-dimensional polymer used since 2006 in heterogeneous catalysis and photocatalysis as a promising material.[27,28,29] From the various allotropic phases that were reported for g-C_3N_4, we have chosen one containing tri-s-triazine (heptazine) rings as a suitable support material, as it can provide not only suitable anchoring holes but also electron lone pairs to trap a metal atom. It is also the most stable phase of C_3N_4 at ambient conditions.[30] From a computational point of view, several studies provide atomistic insight into the interaction of metallic atoms or clusters with ECN supports and their consequences in catalysis.[26,31,32,33,34]

Here, we aim to computationally study, at DFT level, the PDH reaction catalyzed by Pt single-atom catalyst (SAC), Pt_4 single-cluster catalyst (SCC), and the bimetallic cluster Pt_3Sn, all supported on ECN. We performed *ab initio* molecular dynamics (AIMD) simulations to evaluate the stability of the SAC system at common operating temperatures. We then characterize the reaction mechanism of the PDH productive pathway, as well as of the competitive side reactions,

namely deep dehydrogenation and C-C bond breaking, for the different catalytic systems. These energy profiles were used to derive parameters for performing microkinetic modelling of reactivity and selectivity at reaction conditions. Comparing the results obtained for these three catalytic systems allowed gauging the effects of clustering (from Pt_1 to Pt_4) and the addition of promoters such as Sn on the catalytic performance.

COMPUTATIONAL DETAILS

All the calculations were performed using the Vienna Ab Initio Simulation Package (VASP 5.3.5).[35] Projector Augmented Wave (PAW) pseudopotentials were used to describe the core electron density and its interaction with the valence electron density.[36] The exchange-correlation interactions were calculated using the Perdew, Burke, Ernzerhof (PBE) generalized gradient approximation (GGA) functional.[37] This functional adequately describes bulk transition metals in general average terms.[38,39] The van der Waals interactions were considered by the DFT-D3 method of Grimme.[40] Spin-polarization and dipole correction were always included. The cutoff energy of the plane wave basis was set to 400 eV. The residual force and energy convergence criteria were set to 10^{-3} eV/Å and 10^{-5} eV, respectively. The Monkhorst-Pack mesh with a 2×2×1 k-point grid was used to sample the Brillouin zone. A 2×2×1 supercell with 22 Å of vacuum along the z direction was used to avoid unwanted interactions between repeated slabs. A cube of 15×15×15 Å with a k-point grid of 1×1×1 was used for isolated molecules and naked metallic clusters (Pt_1, Pt_4, and Pt_3Sn). The stability of $Pt_1/g\text{-}C_3N_4$ was studied with AIMD simulations using a 4×4×1 supercell and 2×2×1 k-point grid. The AIMD simulations were performed on a microcanonical ensemble from 277 K to 1276 K with a 1.0 fs time-step.

The transition states (TS) searching of elementary reactions started with the climbing-image nudged-elastic-band (CI-NEB) with 5 images and refined with the dimer method. The proper character of the local minima and the TS have been confirmed by vibrational frequencies analysis, ensuring a single imaginary frequency for every TS, and the absence of imaginary frequencies for reactants, intermediates, and products.

In addition, Bader's atoms-in-molecules electronic density analysis[41] was carried out to obtain atomic charges via integration of electronic density within regions delimited by zero flux surfaces, allowing to evaluate the charge transfer between species.

The interaction energy (E_{int}) of Pt_nSn_m (n = 1, 3, 4; m = 0, 1) with the ECN substrate was calculated by (Eq. 1):

$$E_{int} = E_{Pt(n)Sn(m)@C3N4} - (E_{C3N4} + E_{Pt(n)Sn(m)}) \quad (1)$$

where $E_{Pt(n)Sn(m)@C3N4}$ is the energy of the anchored metal on the g-C_3N_4 monolayer. E_{C3N4} and $E_{Pt(n)Sn(m)}$ are the energies of a pristine g-C_3N_4 monolayer and Pt atom, Pt_4 and Pt_3Sn clusters in vacuum, respectively.

The adsorption energy for each adsorbed species is calculated by Eq. 2.

$$E_{ads} = E_{mol\text{-}Pt(n)Sn(m)@C3N4} - (E_{mol} + E_{Pt(n)Sn(m)@C3N4}) \quad (2)$$

where $E_{mol\text{-}Pt(n)Sn(m)@C3N4}$ is the energy of the whole system; E_{mol} stands for the energy of the adsorbed molecule in the gas phase; and $E_{Pt(n)Sn(m)@C3N4}$ is the energy of the catalyst. The energy profiles were made with the reference of propane in the gas phase and the clean surface including the contribution of zero-point energy (ZPE). The ZPEs were computed within the harmonic approximation, considering all the atoms of the system. The Gibbs free energies at a given temperature have been computed according to the methodology described in the electronic supplementary information (ESI).

We have also performed a microkinetic modeling to analyze the PDH process. The rate (r) of the elementary steps in the PDH mechanism was determined by multiplying the coverage of reactants (θ_R) by the corresponding rate coefficient (k), Eq. 3.

$$r = k \cdot \theta_R \tag{3}$$

The rate coefficients were computed following the conventional transition-state theory of Eyring, Evans, and Polanyi, as shown in Eq. 4.[42,43]

$$k = \frac{k_B T}{h} \cdot \frac{Z_{TS}}{Z_{IS}} \cdot e^{-E_a/k_B T} \tag{4}$$

where Z_{IS} and Z_{TS} are the partition functions in the initial and transition states, respectively, E_a is the activation energy with ZPE,[44] T is the temperature, and k_B and h are the Boltzmann and Planck constants, respectively. We have used Eq. 5 to introduce the ZPE contribution in the vibrational partition function. Thus, E_a is the electronic energy, as explained by McQuarrie.[45]

$$Z_{vib} = \prod_i \frac{e^{-h\nu_i/2k_B T}}{1-e^{-h\nu_i/k_B T}} \tag{5}$$

The rate of the adsorption steps was calculated using the classical Hertz-Knudsen equation:

$$r_{ads,i} = P_i (2\pi m_i k_B T)^{-1/2} A_{cat} \theta_i \tag{6}$$

Where p_i is the partial pressure of the gas-phase species i, m_i is the molar mass, and A_{cat} is the area per active site.

This information was used to construct a microkinetic model, which involves solving a system of differential equations representing the reaction network composed of elementary steps, as shown in Table S8. The kinetic equations are described by a system of Ordinary Differential equations (ODEs), which were solved numerically. We employed the open-source Julia Programming Language, using various packages, such as the DifferentialEquations.jl, which provides Rosenbrock methods to solve stiff problems.[46] This type of simulation offers the temporal

evolution of species as a function of initial conditions, including the pressure of reactants and the temperature, like methodologies employed in previous studies.[47]

RESULTS AND DISCUSSION

PDH catalyzed by single-atom $Pt_1/g\text{-}C_3N_4$

The structure of ECN is still controversial, and previous works proposed different types of surface morphologies such as, planar, slightly buckled, or highly corrugated.[48,49] Depending on the lattice parameters, the height along the z-axis within a layer may reach 2.6 Å.[48,49] Here, we have taken a single layer of $g\text{-}C_3N_4$ from the literature with a lattice parameter of 7.123 Å, which is consistent with the experimental value (7.13 Å).[33,34] The modeled $g\text{-}C_3N_4$ monolayer is slightly buckled, with a distance of 1.073 Å between the upper and lower atom along the z direction (see Figure 1). The adsorption mode Pt_1-A is the most stable (E_{int} = -285.6 kJ/mol). In this structure, the Pt atom is placed near the geometric center and in the mean plane of the layer, interacting with two opposite N atoms, in agreement with previous DFT calculations.[4,31]

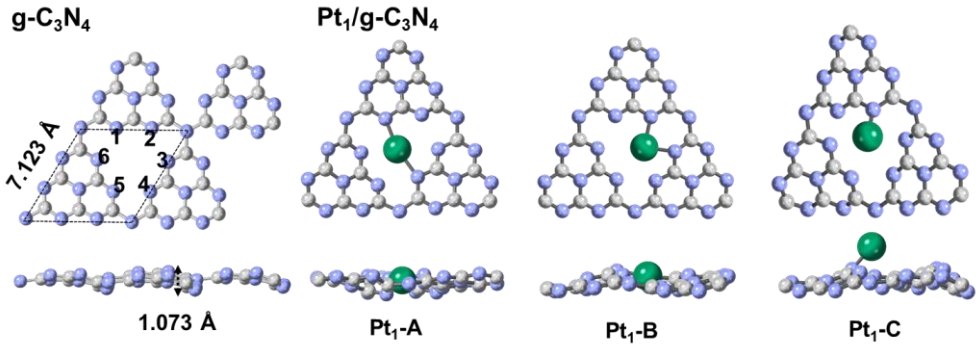

Figure 1. Top and side views of optimized $g\text{-}C_3N_4$ and $Pt_1/g\text{-}C_3N_4$. C, N and Pt are grey, lavender, green, respectively.

As reported by Yang et al,[50] the diffusion barrier between neighbor holes in Pt_1-A configuration is *ca.* 372 kJ/mol as a low limit. Thus, considering the high $E_{int,}$ it is unlikely that the Pt atom will

move between the six-fold cavities along the g-C_3N_4 plane, hindering Pt agglomeration. Two other local minima are found: a configuration Pt_1-B, with Pt forming bonds with two neighbor N atoms and configuration Pt_1-C, connected only to one N atom and shifted 2.115 Å above the average surface plane (Table 1). The configuration Pt_1-C is 40.6 kJ/mol less stable than Pt_1-A, similar to the previously reported value of 47.3 kJ/mol.[31] Since this minimum has an image below the surface, being inactive as catalyst, we modelled this situation with four C_3N_4 layers, like the previous model from Mitchell, López, Pérez-Ramírez *et al.*[34] We have found that the Pt atom has another local minimum between the first and second layers of g-C_3N_4 at 1.66 Å below the first layer and 1.93 Å above the second layer (Figure S7) with a barrier of 41.8 kJ/mol respect to the Pt_1-A position. A close result of 42.5 kJ/mol was reported by López, Pérez-Ramírez *et al.*[31]

Analysis of the electronic structure of the three conformations revealed some significant differences. The Bader charges for configuration Pt_1-A and Pt_1-B are 0.39|e| and 0.55|e|, respectively (Table 1), indicating a significant charge transfer from Pt to linked N atoms. The Bader charge of Pt in configuration Pt_1-C is almost zero, indicating the absence of charge transfer from the metal to the support. Thus, in this configuration the Pt atom is richer in charge, and as will be discussed below, this has consequences on the activity.

Table 1. Different configurations of $Pt_1/g\text{-}C_3N_4$ (Pt_1-A, Pt_1-B and Pt_1-C). E_{int} (kJ/mol) is the interaction energies of Pt_1 with $g\text{-}C_3N_4$. ΔE (kJ/mol) is the relative electronic energy for each configuration concerning the most stable one. Z_{Pt} (Å) refers to the distance between Pt and the average surface plane. Pt-N bond lengths (Å) and Bader charges (|e|) for Pt are also included.

Configuration	E_{int}	ΔE	Z_{Pt}	Pt-N_x bond lengths		Pt charge
Pt_1-A	-285.6	0.0	0.0	Pt-N_1	2.119	0.39
				Pt-N_4	2.230	
Pt_1-B	-275.0	10.6	0.387	Pt-N_2	2.040	0.55
				Pt-N_3	2.011	
Pt_1-C	-245.0	40.6	2.115	Pt-N_2	1.919	0.01

We also analyzed the projected densities of states (pDOS) to gauge the effects on the band structure of the adsorption of Pt atoms at different positions of the $g\text{-}C_3N_4$ support (Figure 2). The bare surface of $g\text{-}C_3N_4$ is a typical semiconductor, the present computed band gap of $g\text{-}C_3N_4$ being 1.6 eV, slightly lower than the experimental value of 2.7 eV.[49] This is unsurprising due to the known underestimation of band gaps using PBE.[51] In configuration Pt_1-B, the orbital mixing between the Pt atom and $g\text{-}C_3N_4$ is large, and there are no d electrons in the band gap. These features suggest that the reactivity of Pt in Pt_1-B configuration is low. In contrast, configurations Pt_1-A and Pt_1-C show d electrons in the band gap, indicating an increase of their reactivity. In addition, configuration Pt_1-C has a band gap that is only 1.2 eV, which results in shift of the Pt d electrons closer to the Fermi level, thereby enhancing its reactivity.

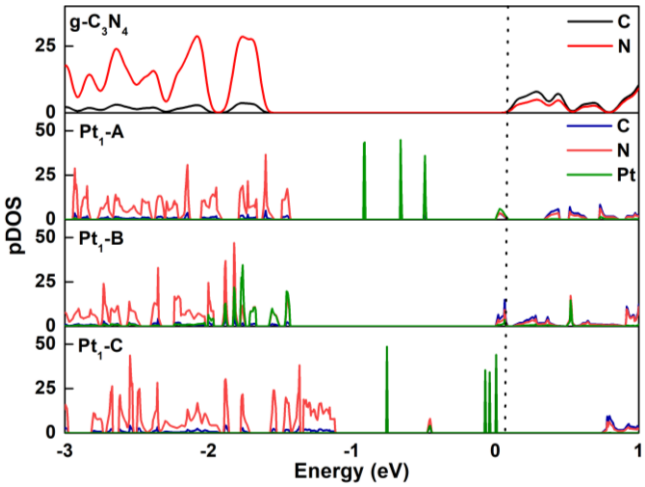

Figure 2. pDOS for g-C_3N_4 (upper) and Pt_1/g-C_3N_4 in Pt_1-A, Pt_1-B, and Pt_1-C configurations. Energy is referred to Fermi level.

The operating temperature of PDH is about 873 K.[6] To evaluate the dynamic stability of the system, we performed AIMD simulations using VASP, in which we gradually increased the temperature from 277 K to 1276 K during a simulation time of 10.0 ps. During the simulations (the Pt atom remains in the hexacyclic cavity, even at high temperatures, fluctuating between Pt_1-A to Pt_1-B and Pt_1-C.

We also determined the energy barriers for the interconversion between the three conformations (Figure 3). The computed energy barriers range from 46.2 to 73.2 kJ/mol, whose values indicate that the three conformations are accessible at working temperatures, in the same line as AIMD simulations. Thus, for the study of PDH mechanism, we will consider the three conformations. However, we anticipate that when propane adsorbs, the conformations Pt_1-A and Pt_1-B lead to the same intermediate A/B-PA* (Table 2).

After analyzing the structure of Pt_1/g-C_3N_4, we characterized the PDH reaction mechanism. The initial stage involves the physisorption of propane and the subsequent C-H activation. In the A/B-PA* intermediate (Table 2), propane interacts weakly with Pt and the C-H bonds involved are only

marginally elongated resulting in a non-reactive intermediate. However, the C-PA* intermediate presents the higher adsorption energy, -61.6 kJ/mol, referred to configuration Pt_1-A and a lengthening of the C-H bond from 1.101 Å to 1.237 Å.

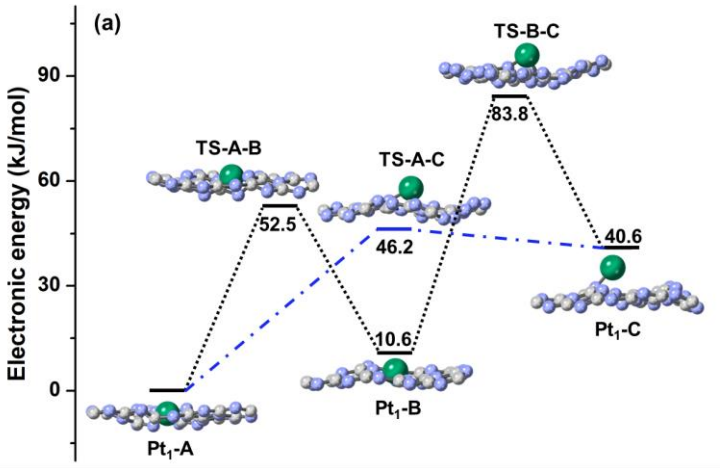

Figure 3. Electronic energy profile, for $Pt_1/g\text{-}C_3N_4$ configurations. C, N, and Pt are grey, lavender, and green, respectively.

Table 2. Adsorbed propane (PA) configurations. Adsorption energies are referred to the most stable configuration of $Pt_1/g\text{-}C_3N_4$, namely configuration Pt_1-A. C, H, N, and Pt are gray, pink, lavender, and green, respectively.

System	Pt_1-A/B-PA*	Pt_1-C-PA*
Configurations (Side View)	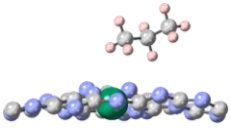	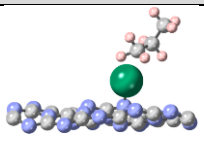
E_{ads} (kJ/mol)	-35.4	-61.6
Pt Bader charge (|e|)	0.39	0.01
C-H distance (Å), gas phase PA	1.100	1.101
C-H distance (Å) PA*	1.100	1.237
Pt-C distance (Å)	3.755	2.248

Based on the above analysis, we propose that the reaction starts at the most stable configuration of the adsorbed propane, Pt_1-C-PA*, from which the C-H bond activation of the primary propane carbon occurs with a small activation energy 14.2 kJ/mol (Figure 4). Note that the energetically favorable propane adsorption state (Pt_1-C-PA*) does not corresponds to the most stable configuration of the bare $Pt_1/g\text{-}C_3N_4$ catalyst (Pt1-A). As Ge *et al.*[52] stated, the global minimum of Pt_n does not necessarily contribute the most to PDH. The initial C-H activation can occur either: via the primary carbon (C_1) or the secondary one (C_2), and the corresponding energy profiles of the reaction pathways are shown in Figure 4 and Figure S1, respectively. The difference in activation energy between the primary and secondary C-H activation is very low (< 4 kJ/mol), within the level of accuracy of our methodology. Therefore, the discussion in the main text will be based on the pathway that initiates by activation of the most abundant (6:2) primary C-H bonds (Figure 4), referring also to the pathway starting by activation of the secondary C-H bonds.

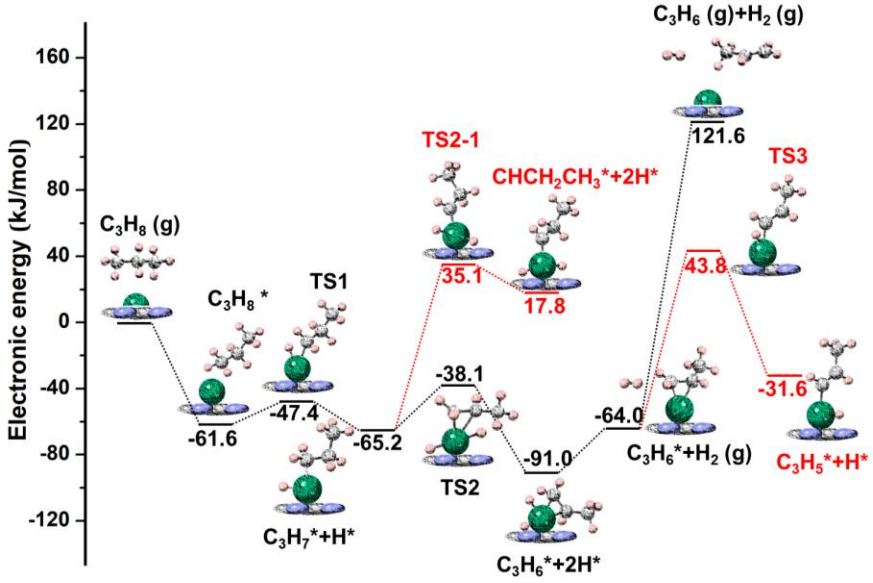

Figure 4. Energy profile of PDH on $Pt_1/g\text{-}C_3N_4$, C_1 adsorption. C, H, N, and Pt are grey, pink, lavender, and green, respectively. Red lines are competing side reaction pathways.

After adsorption, the first C_1-H activation energy is 14.2 kJ/mol (10.9 kJ/mol for C_2). This value is close to that computed for propane C-H activation by atomic Pt^+ (16.4 kJ/mol for C_1 path).[53] Then, the 1-propyl intermediate, C_3H_7* + H* is formed, where both C_1 and H* are bonded to the Pt atom (see Figure 4). We also considered the possibility of C_1 bonded to Pt while H is bonded to a surface terminal nitrogen, as described by Lin, Li, *et al.*,[4] for different transition metals as SAC on g-C_3N_4. However, the H* transfer to g-C_3N_4 support is energetically unfavorable by 39.1 kJ/mol (Table S2). The energy required to cleave the secondary C-H bond at C_3H_7* to give adsorbed propene (C_3H_6* + 2H*) through TS2 is slightly higher than the first C-H activation, with a barrier of 27.1 kJ/mol (37.9 kJ/mol for C_2 pathway). These values are also similar to those reported for the second C-H activation by Pt^+ (34.1 kJ/mol).[53]

Moreover, the C-H bond activations characterized here are closely related to those on Pt surfaces,[8,9,54] or supported Pt_1.[25,55] From C_3H_7* + H*, we characterized a possible side reaction leading to 1-propylidene, $CHCH_2CH_3$*, that can yield deep dehydrogenated products (red lines in Figure 4). Nevertheless, the computed energy barrier for deep dehydrogenation via TS2-1 is 100.3 kJ/mol, significantly higher than the energy barrier for propene formation via TS2 (red lines in Figure 4). Thus, we can discard deep dehydrogenation from the C_3H_7* + H* intermediate.

The final steps of the reaction consist of H_2 formation and desorption, and propene desorption. The desorption of both products goes uphill in energy because of the relatively high adsorption energies of molecular hydrogen and propene on Pt_1, -116.2 kJ/mol and -185.5 kJ/mol, respectively (Table S1). H_2 is likely to desorb first as it has lower E_{ads} than propene. From the C_3H_6* + 2H* intermediate, the energy cost to lead molecular H_2 in gas phase is 27.0 kJ/mol. The propene desorption is significantly more costly, 185.6 kJ/mol, (Figure 4). Moreover, the adsorbed propene can further dehydrogenate to give the 1-propenyl intermediate C_3H_5* through an energy barrier of

107.8 kJ/mol, which is lower than propene desorption but entropically disfavored (see red lines in Figure 4). Thus, the electronic energy is not enough to describe the process; the entropic contribution at high temperatures must be considered (see microkinetic simulations below).

PDH catalyzed by Pt_4 and Pt_3Sn single-clusters

As we have seen, the Pt atoms can diffuse into the bulk of the g-C_3N_4 support, significantly reducing the catalytic activity. Therefore, it is interesting to compare the catalytic performance of Pt_1/g-C_3N_4 with small subnanometric clusters because we move from the limit of high dispersion in SAC, and the clusters can prevent diffusion of Pt into the support. Moreover, subnanometric clusters are usually less active than atomic Pt but present more active sites than bigger clusters or surfaces, thus preventing side reactions.[13,54] Herein, Pt_4 was selected as it provided high activity for methane, ethane, and propane dehydrogenation.[56,57,58] Initially, the optimization of adsorbed Pt_4 was conducted for two possible structures, and both led to the same minimum, a triangular pyramid with the basis pointing to the surface, (Figure 5) with an interaction energy of -417,15 kJ/mol. VASP-AIMD simulations also indicate that the interaction of the Pt_4 cluster with the hole of the g-C_3N_4 surface is stable.

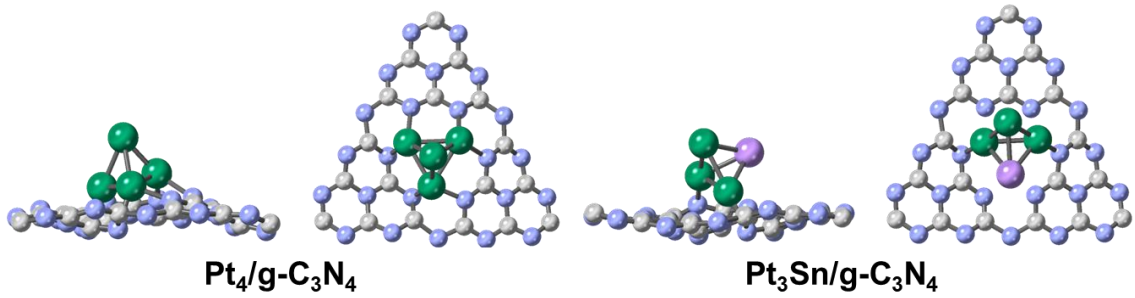

Figure 5. Side and top views of Pt_4/g-C_3N_4 and Pt_3Sn/g-C_3N_4, C, N, Pt, and Sn are grey, lavender, green, and violet, respectively.

Table 3 and Figure 6 show, respectively, the Bader charges of Pt atoms and the pDOS for $Pt_4/g\text{-}C_3N_4$ catalyst. In $Pt_4/g\text{-}C_3N_4$, the Pt atoms interacting with surface via the nitrogen atoms (labeled as 2, 3, and 4, in Table 3) are positively charged due to the charge transfer from Pt to the aromatic rings of the support. In turns, the Pt atom on top of the cluster (labeled as 1) is slightly negatively charged, what in combination with its low coordination, will interact more tightly with propane than the other Pt atoms in the cluster (2, 3, and 4).

Table 3. Bader charges of Pt and Sn for $Pt_4/g\text{-}C_3N_4$ and $Pt_3Sn/g\text{-}C_3N_4$.

System	Side View	Pt_1	Pt_2	Pt_3	Pt_4 or Sn
$Pt_4/g\text{-}C_3N_4$	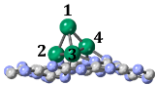	-0.19	0.32	0.31	0.22
$Pt_3Sn/g\text{-}C_3N_4$	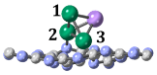	-0.34	-0.02	0.10	0.73

According to the pDOS in Figure 6, the d orbitals of Pt in all the structures (highlighted with circles in Figure 6) are situated within the band gap of the support and act as dopant levels. These d levels of Pt are slightly farther from the Fermi level for $Pt_4/g\text{-}C_3N_4$ than for $Pt_1/g\text{-}C_3N_4\text{-}C$, indicating that $Pt_4/g\text{-}C_3N_4$ is less active than $Pt_1/g\text{-}C_3N_4\text{-}C$. Accordingly, the adsorption energies of propane, propene and hydrogen on $Pt_4/g\text{-}C_3N_4$ are lower than on $Pt_1/g\text{-}C_3N_4$. (Table S1).

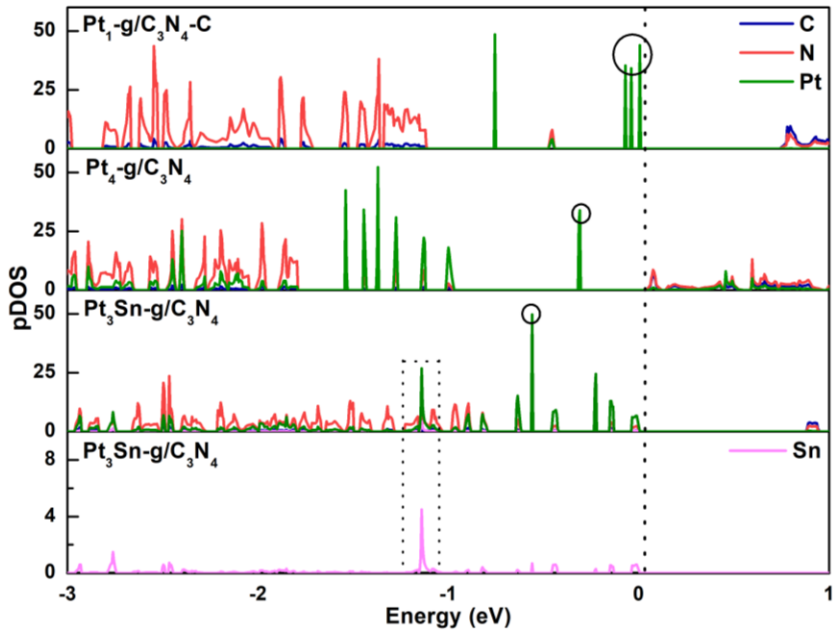

Figure 6. Projected densities of states (pDOS) for $Pt_1/g\text{-}C_3N_4$-C, $Pt_4/g\text{-}C_3N_4$, and $Pt_3Sn/g\text{-}C_3N_4$. Energy is referred to Fermi level.

Figure 7 shows the electronic energy profiles for the mechanism of PDH catalyzed by $Pt_4/g\text{-}C_3N_4$ through the C_1 path, and Figures S2 through the C_2 path. The first C-H bond breaking (25.8 kJ/mol) is higher than on $Pt_1/g\text{-}C_3N_4$, (14.2 kJ/mol), which is consistent with the analysis of the density of states. Compared with Pt(111), $Pt_4/g\text{-}C_3N_4$ is more active, as nearly 70.0 kJ/mol[7,56] are required to initiate the first dehydrogenation of propane on Pt(111) surface. After the first C-H cleavage, the split hydrogen atom, which is bonded to the top Pt atom of the cluster migrates to another Pt atom, forming a more stable intermediate (1^{st} H migration) by a significant amount of energy (see Figure 7 and Table S3). In contrast to $Pt_1/g\text{-}C_3N_4$, the second dehydrogenation is easier than the first one, with a lower energy barrier of 18.8 kJ/mol. The side reaction conducting to propyne formation has a significantly larger energy barrier of 87.5 kJ/mol, indicating that propene is more readily formed than propyne. As a result, C_3H_6* + H* + H* products are formed with one hydrogen adsorbed at the same Pt atom as propene, and the other hydrogen in a different Pt of the

cluster. As it has been reported, the hydrogen atom can diffuse freely with a low barrier on the platinum surface.[58] Thus, we assume that the second H* can migrate to the same Pt atom as the firstly generated H*, allowing H-H bond formation and desorption of molecular H_2. However, H_2 formation and desorption from on the Pt_4 cluster is more difficult than on $Pt_1/g\text{-}C_3N_4$, requiring a substantial energy of 157.5 kJ/mol. The desorption energy of propene from Pt_4 (149.4 kJ/mol) is lower than the one from Pt_1 (185.6 kJ/mol). Yet, the barrier for deep dehydrogenation (68.1 kJ/mol), is still lower than for desorption and even lower than for $Pt_1/g\text{-}C_3N_4$ (107.8 kJ/mol). However, the difference between the desorption energy and deep dehydrogenation barrier for $Pt_1/g\text{-}C_3N_4$ and $Pt_4/g\text{-}C_3N_4$ is similar, with values of about 80 kJ/mol. To sum up, the propane activation is faster for $Pt_4/g\text{-}C_3N_4$ than for $Pt_1/g\text{-}C_3N_4$, but the desorption of propene is still energetically costly.

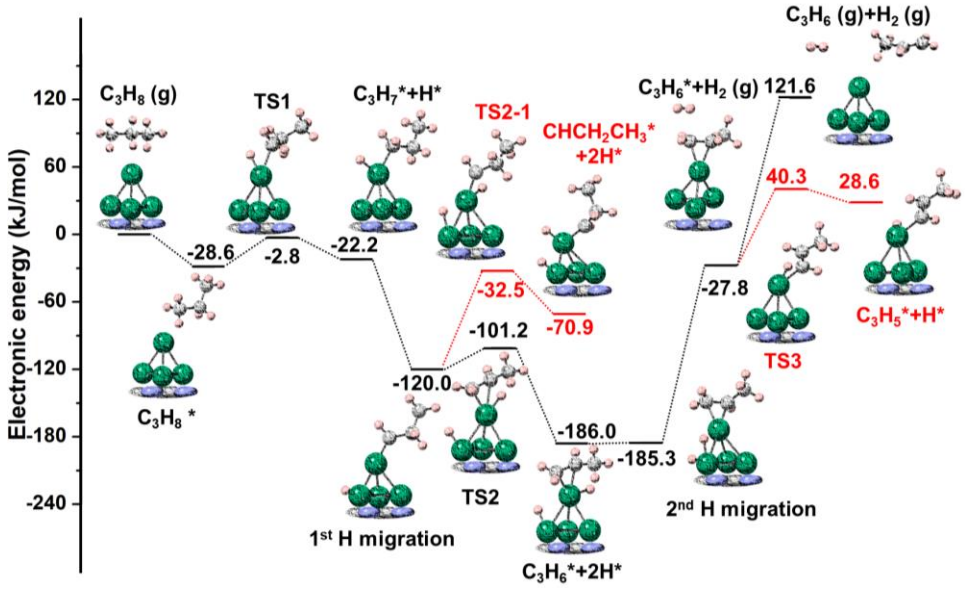

Figure 7. Energy profile of PDH on $Pt_4/g\text{-}C_3N_4$, C_1 adsorption. C, H, N, and Pt are grey, pink, lavender, and green, respectively. Red lines are the competing side reaction pathways.

We then investigate the PDH mechanism on the Pt_3Sn cluster as a model for subnanometrized PtSn alloy clusters, since PtSn catalysts have been shown to increase selectivity towards

propene.[15,58,59,60] The Sn atom occupies some of the active sites of Pt clusters, reducing side reactions.[15] Moreover, a substantial charge transfer between Sn and Pt can shift the d-band center of Pt downwards, favoring the desorption of products.[13,61,62] To this end we evaluated all possible configurations of the Pt_3Sn cluster adsorbed on the g-C_3N_4 surface. The most stable structure, with an interaction energy of -338.1 kJ/mol, corresponds to two Pt atoms that coordinate with two different nitrogen atoms of the support, while the other Pt and Sn atom point upwards, out of the surface, forming a tetrahedron-like structure (Figure 5). In Pt_3Sn/g-C_3N_4, the Pt atom non-interacting with the surface (Pt_1) carries more negative charge than the Pt atoms in Pt_4/g-C_3N_4 because the Sn atom transfers additional charge to its Pt neighbors (Table 3). As a result, the d band center of Pt_3Sn/g-C_3N_4 is shifted downward, indicating a reduction in the reactivity of the surface. In the pDOS representation for Pt_3Sn/g-C_3N_4, Figure 6, it is more difficult to distinguish the band gap, but compared with Pt_4/g-C_3N_4, the unoccupied d electrons are farther from the Fermi level. The role of Sn therefore consists in tuning the reactivity of Pt by broadening the d-band of Pt (Figure 6) and reducing the activity.[57,58] The adsorption energies on Pt_3Sn/g-C_3N_4 of the key species involved in PDH are collected in Table S1. Previous studies have shown that they adsorb preferentially on the Pt atoms because they are electron-rich compared to Sn atoms (Table 3).[59,63] The adsorption energy of propane is similar to that on Pt_4. In contrast, propene and hydrogen adsorption energies on Pt_3Sn are lower than on Pt_4.

The electronic energy profiles of PDH on Pt_3Sn/g-C_3N_4 through C_1 and C_2 pathways are given in Figure 8 and Figure S3, respectively. The energy barrier to reach the first transition state, corresponding to the activation of the primary C-H bond of propane, is 65.0 kJ/mol higher than that on Pt_4/g-C_3N_4 (25.8 kJ/mol). Interestingly, the introduction of Sn has little effect on the secondary C-H bond breaking; the barrier is 5.2 kJ/mol, even smaller than the18.8 kJ/mol for Pt_4/g-

C_3N_4. The barrier for the side reaction yielding deep dehydrogenation of the primary carbon (TS2-1 on Pt_3Sn, 75.2 kJ/mol) is much higher than that for the secondary C-H activation to give the adsorbed propene (TS2 on Pt_3Sn, 5.2 kJ/mol). For the first and second intermediates (C_3H_7* + H* and C_3H_6* + 2H*), all possible structures are shown in Tables S5 and S6, respectively. For C_3H_7* + H*, the 1st migration of H* to another Pt atom is energetically favorable similar to that found for Pt_4/g-C_3N_4. For the next step, C_3H_6* + 2H* with 2nd H migration, the most stable configuration places the two adsorbed H* on different Pt atoms, unlike for Pt_4/g-C_3N_4. This means that additional energy (27.3 kJ/mol) is necessary to bring the two hydrogen atoms to the same Pt atom to allow H_2 formation and desorption (entry 3 in Table S6, and the 3rd H migration in Figure 8). Furthermore, unlike Pt_4 (Table S4), we found a di-σ adsorption mode of propene bridging two Pt atoms (entry 7 in Table S6), which is only 11.0 kJ/mol higher than the lowest π configuration of C_3H_6* + 2H* with the 2nd H migration atoms (entry 2 in Table S6). The lowest energy barrier was found for the most stable π adsorption mode, 5.2 kJ/mol (Figure8). Finally, for Pt_3Sn/g-C_3N_4, both hydrogen and propene desorption are large, 84.6 and 141.2 kJ/mol, respectively, but less unfavorable than for Pt_4 cluster. The barrier for deep dehydrogenation from adsorbed propene C_3H_6* (111.5 kJ/mol) is comparable to the desorption energy of propene. All in all, these results indicate that Pt_3Sn/g-C_3N_4 would be less reactive toward C-H activation than Pt_4/g-C_3N_4, but the easier desorption would prevent side reactions such as deep dehydrogenation and C-C bond breaking, improving the selectivity.

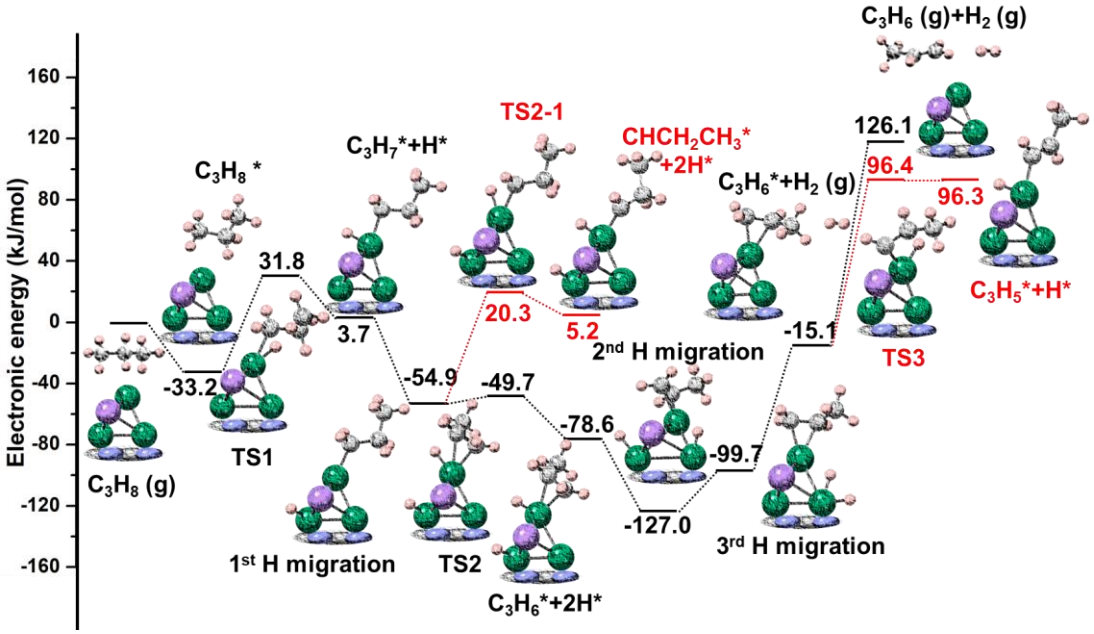

Figure 8. Energy profile of PDH on $Pt_3Sn/g\text{-}C_3N_4$, C_1 adsorption. C, H, N, Pt and Sn, are grey, pink, lavender, green and violet, respectively. Red lines are the competing side reaction pathways.

Gibbs free energy profiles and microkinetic analysis

Further analysis was conducted to make the simulation closer to the operating conditions. The calculated temperature dependence of the Gibbs free energy reaction for PDH, compared with that obtained from experimental data, is shown in Figure S5, the difference being less than 10 kJ/mol. The free energy reaction decreases with increasing temperature, and becomes exergonic at about 873 K, usually taken as the working temperature. Free energy profiles at 873 K (Figure 9 and Figure S6 for C_1 and C_2 respectively) are given for the three catalysts. The results show, as expected, that while temperature has a significant impact on adsorption and desorption, it has a relatively small effect on C-H bond activation barriers.

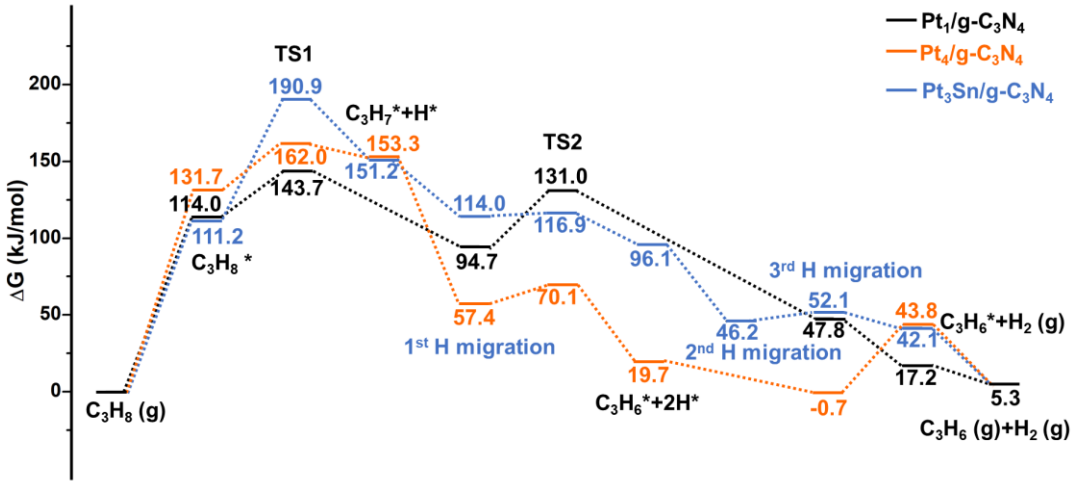

Figure 9. PDH free energy profiles on $Pt_1/g\text{-}C_3N_4$, $Pt_4/g\text{-}C_3N_4$ and $Pt_3Sn/g\text{-}C_3N_4$, at 873 K for C_1 adsorption.

The single-atom $Pt_1/g\text{-}C_3N_4$ system is the most active with an overall free-energy barrier (energy span) of 143.7 kJ/mol corresponding to the energy required to reach the transition state for the first C-H activation (TS1 for $Pt_1/g\text{-}C_3N_4$, see Figure 9). The same process determines the energy span for Pt_4 and Pt_3Sn catalysts, the overall free-energy barrier being higher for Pt_4 than for Pt_1 but lower than for Pt_3Sn. We also note that the desorption of H_2 in $Pt_4/g\text{-}C_3N_4$ is more difficult because the C_3H_6* + H* + H* (2nd H migration step) forms a relatively deep energy well. $Pt_3Sn/g\text{-}C_3N_4$ facilitates the desorption process, but the activation of a third C-H bond is more energy demanding (Table S7). Therefore, side reactions and deep dehydrogenation are less likely to occur on Pt_3Sn.

All the previously considered reactions were included in the microkinetic analysis (Table S8). In addition, as the initially inactive Pt_1-A, has to move to Pt_1-C, and the Pt atom can also move below the first layer deactivating the catalyst, we included the corresponding elementary steps (Figure 3 and Figure S7). The conversion of propane is reported with and without considering the

Pt diffusion into the support at 873.15 K (Figure 10). The $Pt_1/g\text{-}C_3N_4$ catalyst is the most active without considering Pt diffusion, close to Pt_3Sn. However, if the diffusion of Pt below the surface is considered, the activity of $Pt_1/g\text{-}C_3N_4$ is significantly reduced, and becomes even less active than $Pt_4/g\text{-}C_3N_4$. Pt_4 is less performant than the others because it favors deep dehydrogenation, which leads to coke formation. This is evidenced by the fact that the 2-propenylidene species on $Pt_4/g\text{-}C_3N_4$ is more than 6 orders of magnitude higher than on the other catalytic systems. It is important to note that, although the velocities are different, all catalysts reached equilibrium conversion at 873.15 K, *ca*. 32%.

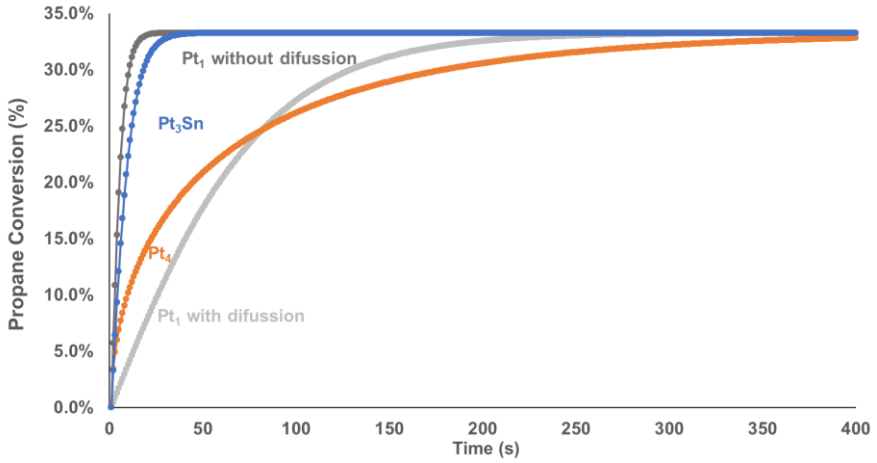

Figure 10. Predicted propane conversion on $Pt_1/g\text{-}C_3N_4$, $Pt_4/g\text{-}C_3N_4$, and $Pt_3Sn/g\text{-}C_3N_4$, at 873.15 K, 1atm.

Figure 11 shows the evolution of propane conversion over time at different temperatures. It shows that Pt_3Sn has the highest conversion and can reach the equilibrium at all temperatures; Pt_1 (taking diffusion into account) has a better conversion than Pt_4 when the temperature is below 873.15 K, but the trend is reversed at high T because the diffusion of Pt_1 below the first surface layer increases.

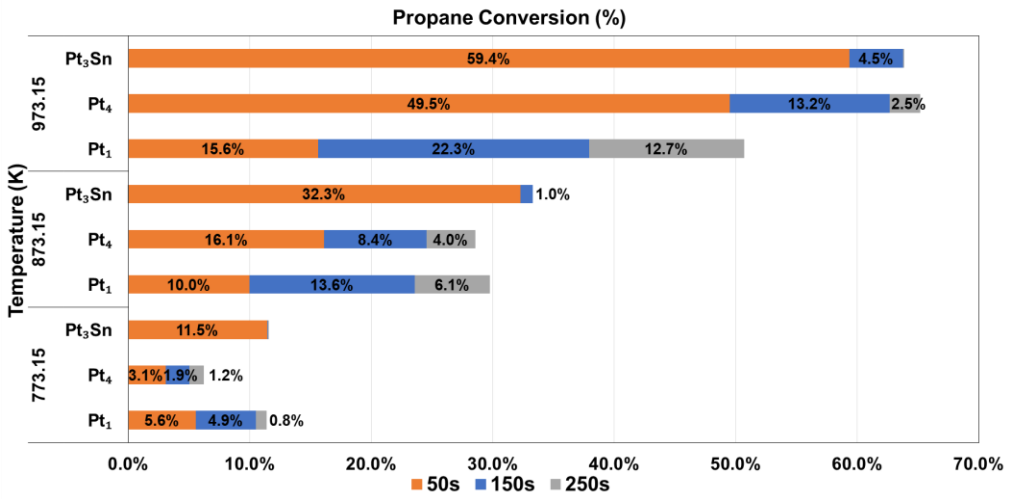

Figure 11. Predicted propane conversion on $Pt_1/g\text{-}C_3N_4$, $Pt_4/g\text{-}C_3N_4$, and $Pt_3Sn/g\text{-}C_3N_4$, at different times (59, 150, 250 s) and temperatures (773.15 - 973.15 K).

The analysis at different temperatures can also be used to estimate the apparent activation energy of the reaction. To build the Arrhenius plot, we calculated the reactive velocity at initial times. This satisfied the linearity of the Arrhenius plot. The apparent activation energies were found to be 31, 57 and 34 kJ/mol for $Pt_1/g\text{-}C_3N_4$, $Pt_4/g\text{-}C_3N_4$ and $Pt_3Sn/g\text{-}C_3N_4$ catalysts, respectively. These estimations are in the same order than the values obtained by Sui, Chen, *et al.*[12] for PDH on Pt/Al_2O_3 nanocatalyst, 56 kJ/mol on small clusters and 26 kJ/mol on atomically dispersed Pt.

CONCLUSIONS

In summary, three Pt-based catalysts for PDH were theoretically designed and compared: single-atom ($Pt_1/g\text{-}C_3N_4$) and single clusters ($Pt_4/g\text{-}C_3N_4$ and $Pt_3Sn/g\text{-}C_3N_4$). All these systems were found to be active for PDH. The initial propane adsorption and C-H activation of the primary bond follows the reactivity order: $Pt_1 > Pt_4 > Pt_3Sn$. In the most reactive $Pt_1/g\text{-}C_3N_4$ catalyst, the low coordinated Pt atom adsorbs better the propane substrate facilitating the subsequent activation. On the other hand, the rate of propene desorption, which have been related with the PDH selectivity,

follows the opposite trend: Pt_1 < Pt_4 < Pt_3Sn. In $Pt_3Sn/g\text{-}C_3N_4$ catalyst, the easiest propene desorption and the highest barrier for deep dehydrogenation in C_3H_6* state among the studied systems indicate that this is the most selective catalyst. Besides these general trends in PDH, our atomistic simulations have revealed other effects that influence the overall activity/selectivity of the catalytic process. In the single atom catalyst $Pt_1/g\text{-}C_3N_4$, the Pt atom can diffuse below the surface of the support at working temperature conditions, causing catalytic deactivation. Contrary to extended solids, in single-atom or subnanometric clusters, the hydrogen produced after dehydrogenation cannot diffuse along extended surfaces and this can have consequences on the relative energies of intermediate species. Here, we observed a relative, deep energy well for $Pt_4/g\text{-}C_3N_4$ catalyst, reducing its overall activity. The microkinetic analysis shows that the propane conversion on $Pt_3Sn/g\text{-}C_3N_4$ and $Pt_1/g\text{-}C_3N_4$ are comparable; however, if the diffusion of Pt atoms below the top layer is considered, the activity of Pt_1 drops sharply and becomes even lower than that of $Pt_4/g\text{-}C_3N_4$ catalyst. The low activity of $Pt_4/g\text{-}C_3N_4$ is caused by the coverage of active sites by deep dehydrogenated species, which is suppressed in $Pt_3Sn/g\text{-}C_3N_4$ due to easier desorption of propene at working conditions, thus making this one the best catalyst for PDH among the systems studied here. Overall, these Pt-based catalysts, supported on $g\text{-}C_3N_4$, offer a promising direction for the development of PDH, providing important insights for future research.

ASSOCIATED CONTENT

Supporting Information.

The supporting information include details on the thermodynamic calculations, additional tables and figures for the relevant structures and the C_2 pathways. (PDF)

Data set collections of the computed structures are available in the NOMAD[64] (gP9aZpx0Rg-d6B5YH6YxqA) and ioChem-BD[65] (DOI: 10.19061/iochem-bd-2-73) repositories.

AUTHOR INFORMATION

Corresponding Authors

Josep M. Ricart, Departament de Química Física i Inorgànica, Universitat Rovira i Virgili, Tarragona, Spain. E-mail: josep.ricart@urv.cat.

Present Addresses

Evgenii Strugovschikov, Université de Lorraine, CNRS, LEMTA, Nancy F-54000, France. E-mail: evgenii.strugovshchikov@univ-lorraine.fr

Author Contributions

The manuscript was written through contributions of all authors. All authors have given approval to the final version of the manuscript.

ACKNOWLEDGMENTS

This work has been performed as part of a Joint Research Agreement between TotalEnergies OneTech Belgium (Contract IPA-6119). We thank grants PID2021-128128NB-I00 and PID2023-147292OB-I00. funded by MICIU/AEI/10.13039/501100011033 and by ERDF/EU and the Generalitat de Catalunya (2021SGR00110 and 2021SGR00163). J. P. thanks AGAUR from the Generalitat de Catalunya for the grant 2020-FISDU-00174.

REFERENCES

(1) Lavrenov, A. V.; Saifulina, L. F.; Buluchevskii, E. A.; Bogdanets, E. N. Propylene Production Technology: Today and Tomorrow. *Catal. Ind.* **2015**, *7*, 175-187, DOI: 10.1134/S2070050415030083

(2) Feng, B.; Wei, Y. C.; Song, W. Y.; Xu, C. M. A review on the structure-performance relationship of the catalysts during propane dehydrogenation reaction. *Pet. Sci.* **2022**, *19*, 819-838, DOI: 10.1016/j.petsci.2021.09.015

(3) Bhasin, M. M.; McCain, J. H.; Vora, B. V.; Imai, T.; Pujadó, P. R. Dehydrogenation and oxydehydrogenation of paraffins to olefins. *Appl. Catal. A Gen.* **2001**, *221*, 397-419, DOI: 10.1016/S0926-860X(01)00816-X

(4) Kong, N.; Fan, X.; Liu, F.; Wang, L.; Lin, H.; Li, Y.; Lee, S. T. Single Vanadium Atoms Anchored on Graphitic Carbon Nitride as a High Performance Catalyst for Non-oxidative Propane Dehydrogenation. *ACS Nano* **2020**, *14*, 5772-5779, DOI: 10.1021/acsnano.0c00659

(5) Wang, H. M.; Chen, Y.; Yan, X.; Lang, W. Z.; Guo, Y. J. Cr doped mesoporous silica spheres for propane dehydrogenation in the presence of CO_2: Effect of Cr adding time in sol-gel process. *Microporous and Mesoporous Mater.* **2019**, *284*, 69-77, DOI: 10.1016/j.micromeso.2019.04.016

(6) Chen, S.; Chang, X.; Sun, G.; Zhang, T.; Xu, Y.; Wang, Y.; Pei, C.; Gong, J. Propane dehydrogenation: catalyst development, new chemistry, and emerging technologies. *Chem Soc Rev.* **2021**, *50*, 3315-3354, DOI: 10.1039/d0cs00814a

(7) Zhao, Z. J.; Chiu, C. C.; Gong, J. Molecular understandings on the activation of light hydrocarbons over heterogeneous catalysts. *Chem Sci*. **2015**, *6*, 4403-4425, DOI: 10.1039/c5sc01227a

(8) Saerens, S.; Sabbe, M. K.; Galvita, V. V.; Redekop, E. A.; Reyniers, M. F.; Marin, G. B. The Positive Role of Hydrogen on the Dehydrogenation of Propane on Pt(111). ACS Catal. **2017**, 7, 7495-7508, DOI: 10.1021/acscatal.7b01584

(9) Salóm-Català, A.; Strugovshchikov, E.; Kaźmierczak, K.; Curulla-Ferré, D.; Ricart, J. M.; Carbó, J. J. Reactive Force Field Development for Propane Dehydrogenation on Platinum Surfaces. *J. Phys. Chem C* **2024**, *128*, 2844-2855, DOI: 10.1021/acs.jpcc.3c07126

(10) Fricke, C.; Rajbanshi, B.; Walker, E. A.; Terejanu, G.; Heyden, A. Propane Dehydrogenation on Platinum Catalysts: Identifying the Active Sites through Bayesian Analysis. *ACS Catal.* **2022**, *12*, 2487−2498, DOI: 10.1021/acscatal.1c04844

(11) Yang, M. L.; Zhu, Y. A.; Fan, C.; Sui, Z. J.; Chen, D.; Zhou, X. G. DFT study of propane dehydrogenation on Pt catalyst: effects of step sites. *Phys. Chem. Chem. Phys.* **2011**, *13*, 3257-3267, DOI: 10.1039/c0cp00341g

(12) Zhang, W.; Wang, H.; Jiang, J.; Sui, Z.; Zhu, Y.; Chen, D.; Zhou, X. Size Dependence of Pt Catalysts for Propane Dehydrogenation: from Atomically Dispersed to Nanoparticles. *ACS Catal*. **2020**, *10*, 12932-12942, DOI: 10.1021/acscatal.0c03286

(13) Lian, Z.; Ali, S.; Liu, T.; Si, C.; Li, B.; Su, D. S. Revealing Janus character of the coke precursor in the propane direct dehydrogenation on Pt catalysts from the kMC simulation. *ACS Catal*. **2018**, *8*, 4694-4704, DOI: 10.1021/acscatal.8b00107

(14) Batzill, M.; Beck, D. E.; Koel, B. E. Electronic contrast in scanning tunneling microscopy of Sn-Pt(111) surface alloys. *Surf. Sci.* **2000**, *466*, L821-L826, DOI: 10.1016/S0039-6028(00)00803-7

(15) Zhang, J.; Deng, Y.; Cai, X.; Chen, Y.; Peng, M.; Jia, Z.; Jiang, Z.; Ren, P.; Yao, S.; Xie, J.; Xiao, D.; Wen, X. D.; Wang, N.; Liu, H.; Ma, D. Tin Assisted Fully Exposed Platinum Clusters Stabilized on Defect-Rich Graphene for Dehydrogenation Reaction. *ACS Catal.* **2019**, *9*, 5998-6005, DOI: 10.1021/acscatal.9b00601

(16) Zhang, T. Single-Atom Catalysis: Far beyond the Matter of Metal Dispersion. *Nano Lett.* **2021**, *21*, 9835-9837, DOI: 10.1021/acs.nanolett.1c02681

(17) Qiao, B.; Wang, A.; Yang, X.; Allard, L.; Jiang, F. Z.; Cui, Y.; Liu, J.; Li, J.; Zhang, T. Single-atom catalysis of CO oxidation using Pt_1/FeO_x. *Nat. Chem.* **2011**, *3*, 634-641, DOI: 10.1038/NCHEM.1095

(18) Zhai, Z.; Zhang, B.; Wang, L.; Zhang, X.; Liu, G. Tailoring the catalytic performance of single platinum anchored on graphene by vacancy engineering for propane dehydrogenation: a theoretical study. *Phys. Chem. Chem. Phys*. **2021** *23*, 22004-22014, DOI: 10.1039/d1cp02631c

(19) Mitchell, S.; Pérez-Ramírez, J. Single atom catalysis: a decade of stunning progress and the promise for a bright future. *Nat. Comm.* **2021**, *11*, 4302-4304, DOI: 10.1038/s41467-020-18182-5

(20) Mitchell, S.; Vorobyeva, E.; Pérez-Ramírez, J. The Multifaceted Reactivity of Single-Atom Heterogeneous Catalysts. *Angew. Chem.* **2018**, *57*, 15316-15329, DOI: 10.1002/anie.201806936

(21) Kumar, P.; Al-Attas, T. A.; Hu, J.; Kibria, Md. G. Single Atom Catalysts for Selective Methane Oxidation to Oxygenates. *ACS Nano* **2022**, *16*, 8557-8681, DOI: 10.1021/acsnano.2c02464

(22) Yang, X. F.; Wang, A.; Quiao, B.; Li, J.; Liu, J.; Zhang, T. Single-Atom Catalysts: A New Frontier in Heterogeneous Catalysis. *Acc. Chem. Res.* **2013**, *46*, 1740-1748, DOI: 10.1021/ar300361m

(23) Zhuo, H. - Y.; Zhang, X.; Xia, J.; Yu, Q.; Xiao, H.; Li, J. Theoretical Understandings of Graphene-based Metal Single-Atom Catalysts: Stability and Catalytic Performance. *Chem. Rev.* **2020**, *120*, 12315-12341, DOI: 10.1021/acs.chemrev.0c00818

(24) Liu, X.; Sui, Y.; Duan, T.; Meng, C.; Han, Y. CO Oxidation catalyzed by Pt-embedded graphene: a first-principles investigation. *Phys. Chem. Chem. Phys*. **2014**, *16*, 23584-23593, DOI: 10.1039/c4cp02106a

(25) Zhai, Z.; Zhang, B.; Wang, L.; Zhang, X.; Liu, G. Tailoring the catalytic performance of single platinum anchored on graphene by vacancy engineering for propane dehydrogenation: a theoretical study. *Phys. Chem. Chem. Phys*. **2021**, *23*, 22004-22013, DOI: 10.1039/D1CP02631C

(26) Vilé, G.; Albani, D.; Nachtegaal, M.; Chen, Z.; Dontsova, D.; Antonietti, M.; López N.; Pérez-Ramírez, J. A Stable Single-Site Palladium Catalyst for Hydrogenations. *Angew. Chem*. **2015**, *54*, 11265-11269, DOI: 10.1002/anie.201505073

(27) Goettmann, F.; Fischer, A.; Antonietti, M.; Thomas, A. Chemical Synthesis of Mesoporous Carbon Nitrides Using Hard Templates and Their Use as a Metal-Free Catalyst for Friedel-Crafts Reaction of Benzene. *Angew. Chem.* **2006**, *45*, 4467-4471, DOI: 10.1002/anie.200600412

(28) Ong, W. J.; Tan, L. L.; Ng, Y. H.; Yong, S. T.; Chai, S. P. Graphitic Carbon Nitride ($g\text{-}C_3N_4$)-Based Photocatalysts for Artificial Photosynthesis and Environmental Remediation: Are We a Step Closer To Achieving Sustainability. *Chem*. *Rev*. **2016**, *116*, 7159-7329, DOI: 10.1021/acs.chemrev.6b00075

(29) Rocha, G. F. S. R.; da Silva, M. A. R.; Rogolino, A. A. D; Noleto, L. F. G.; Antonietti M.; Teixeira, I. F. Carbon Nitride-based Materials: More than just a Support for Single-atom Catalysis. *Chem. Soc. Rev.* **2023**, *52*, 4878-4934, DOI: 10.1039/d2cs00806h

(30) Zheng, Y.; Lin, L.; Wang, B.; Wang, X. Graphitic Carbon Nitride Polymers toward Sustainable Photoredox Catalysis. *Angew. Chem.* **2015**, *54*, 12868-12884, DOI: 10.1002/anie.201501788

(31) Chen, Z.; Mitchell, S.; Vorobyeva, E.; Leary, R. K.; Hauert, R.; Furnival, T.; Ramasse, Q. M.; Thomas, J. M.; Midgley, P. A.; Dontsova, D.; Antonietti, M.; Pogodin, S.; López. N.; Pérez-Ramírez, J. Stabilization of Single Metal Atoms on Graphitic Carbon Nitride. *Adv. Funct. Mater.* **2017**, *27*, 1605785-1605797, DOI: 10.1002/adfm.201605785

(32) Yang, Y.; Wang, J.; Lin, H.; Dong, H.; Li, Y. On-purpose Design of Dual Active Sites in single V atom anchored C_2N nanosheets for Propane Dehydrogenation catalysis. *Inorg. Chem. Front.* **2022**, *9*, 5517-5526, DOI: 10.1039/d2qi01463g

(33) Chen, Z.; Vorobyeva, E.; Mitchell, S.; Fako, E.; Ortuño, M. A.; López, N.; Collins, S. M.; Midgley, P. A.; Richard, S.; Vilé, G.; Pérez-Ramírez, J. A Heterogeneous Single-atom Palladium Catalyst Surpassing Homogeneous Systems for Suzuki Coupling. *Nat. Nanotechnol.* **2018**, *13*, 702-707, DOI: 10.1038/s41565-018-0167-2

(34) Vorobyeva, E.; Fako, E.; Chen, Z.; Collins, S. M.; Johnstone, D.; Midgley, P. A.; Hauert, R.; Safonova, O. V.; Vilé, G.; López, N.; Mitchell, S.; Pérez-Ramírez, J. Atom-by-Atom Resolution of Structure-Function Relations over Low-Nuclearity Metal Catalysts. *Angew. Chem.* **2019**, *131*, 8816-8821, DOI: 10.1002/anie.201902136

(35) Kresse, G.; Furthmüller, J. Efficient iterative Schemes for Ab initio Total-energy Calculations Using a Plane-wave Basis Set. *Phys. Rev. B* **1996**, *54*, 11169-11186, DOI: 10.1103/physrevb.54.1116

(36) Blöchl, P. E. Projector Augmented-wave Method. *Phys. Rev. B.* **1994**, *50*, 17953-17979, DOI: 10.1103/PhysRevB.50.17953

(37) Perdew, J. P.; Burke, K.; Ernzerhof, M. Generalized Gradient Approximation Made Simple. *Phys. Rev. Lett*. **1996**, *77*, 3865-3868, DOI: 10.1103/PhysRevLett.77.3865

(38) Vega, L.; Martínez, B.; Viñes, F.; Illas, F. Robustness of Surface Activity Electronic Structure-based Descriptors of Transition Metals. *Phys.Chem.Chem.Phys.* **2018**, *20*, 20548-20554, DOI: 10.1039/c8cp03356k

(39) Di Liberto, G.; Cipriano, L. C.; Pacchioni, G. Universal Principles for the Rational Design of Single Atom Electrocatalysts? Handle with Care. *ACS Catal.* **2022**, *12*, 5846-5856, DOI: 10.1021/acscatal.2c01011

(40) Grimme, S.; Antony, J.; Ehrlich, S.; Krieg, H. A Consistent and Accurate Ab Initio Parametrization of Density Functional Dispersion Correction (DFT-D) for the 94 elements H-Pu. *J. Chem. Phys.* **2010**, *132*, 154104-154124, DOI: 10.1063/1.3382344

(41) Bader, R. F. W. Atoms in Molecules: A Quantum Theory; Oxford University Press: Oxford, UK, 1990

(42) Eyring, H. The Activated Complex in Chemical Reactions. *J. Chem. Phys.* **1935**, *3*, 107-117, DOI: 10.1063/1.1749604

(43) Evans, M. G.; Polanyi, M. Some Applications of the Transition State Method to the Calculation of Reaction Velocities, Especially in Solution. *Trans. Faraday Soc.* **1935**, *31*, 875-895, DOI: 10.1039/TF9353100875

(44) Laidler, K. J. *Chemical Kinetics* Harper Collins: New York, 1987

(45) McQuarrie, D. A.; Simon, J. D. *Molecular Thermodynamics*, University Science Books, Sausalito, 1999

(46) Bezanson, J.; Edelman, A.; Karpinski, S.; Shah, V. B. Julia: A Fresh Approach to Numerical Computing. *SIAM Rev.* **2017**, *59*, 65-98, DOI: 10.1137/141000671

(47) Roldán, A.; Novell-Leruth, G.; Ricart, J. M.; Illas F. Pt(100) Theoretical Simulation of Temperature Programmed Desorption of Molecular Oxygen on Isolated Au Nanoparticles from density Functional Calculations and Microkinetics Models. *J. Phys. Chem. C* **2010**, *114*, 5101-5106, DOI: 10.1021/jp911283j

(48) Gracia, J.; Kroll, P. Corrugated Layered Heptazine-based Carbon Nitride: the Lowest Energy Modifications of C_3N_4 ground State. *J. Mater. Chem.* **2009**, *19*, 3013-3019, DOI: 10.1039/b821568e

(49) Azofra, L. M.; MacFarlane, D. R.; Sun, C. A DFT Study of Planar vs. Corrugated Graphene like Carbon Nitride (g-C_3N_4) and its Role in the Catalytic Performance of CO_2 Conversion. *Phys. Chem. Chem. Phys*. **2016**, *18*, 18507-18514, DOI: 10.1039/c6cp02453j

(50) Yang, C.; Zhao, Z.; Liu, Q. Mechanistic Insight into the Dispersion Behavior of Single Platinum Atom on Monolayer g-C_3N_4 in Single-atom Catalysts from Density Functional Theory Calculations. *App. Surf. Sci.* **2021**, *566*, 150697-150706, DOI: 10.1016/j.apsusc.2021.150697

(51) Ong, K. P.; Bai, K.; Blaha, P.; Wu, P. Electronic Structure and Optical Properties of $AFeO_2$ (A = Ag, Cu) within GGA Calculations. *Chem. Mater.* **2007**, *19*, 634-640, DOI: 10.1021/cm062481c

(52) Shore, T. C.; Mith, D.; Deprekel, D.; McNall, S.; Ge, Y. A B3LYP study on the C-H Activation in Propane by Neutral and +1 Charged Low-energy Platinum Clusters with 2-6 Atoms. *Reac. Kinet. Mech. Cat.* **2013**, *109*, 315-333, DOI 10.1007/s11144-013-0572-3

(53) Liu, Z.; Li, Z.; Li, G.; Wang, Z.; Lai, C.; Wang, X.; Pidko, E. A.; Xiao, C.; Wang, F.; Li, G.; Yang, X.; Single-Atom Pt^+ Derived from the Laser Dissociation of a Platinum Cluster: Insights into Nonoxidative Alkane Conversion. *J. Phys. Chem. Lett*. **2020**, *11*, 5987-5991, DOI: 10.1021/acs.jpclett.0c01416

(54) Yang, M. - L.; Zhu, J.; Zhu, Y - A.; Sui, Z. - J.; Yu, Y. - D.; Zhou, X.- G.; Chen, D.; Tuning Selectivity and Stability in Propane Dehydrogenation by Shaping Pt Particles: A Combined Experimental and DFT Study. *J. Mol Cat. A* **2014**, *395*, 329-336, DOI: 10.1016/j.molcata.2014.08.008

(55) Sun, X.; Liu, M.; Huang, Y.; Li, B.; Zhao, Z.; Electronic Interaction Between Single Pt tom and Vacancies on Boron Nitride Nanosheets and its Influence on the Catalytic Performance in the

Direct Dehydrogenation of Propane. *Chin. J. Catal.* **2019**, *40*, 819-825, DOI: 10.1016/S1872-2067(18)63196-1

(56) Xiao, L.; Wang, L.; Methane Activation on Pt and Pt4: A Density Functional Theory Study. *J. Phys.Chem. B* **2007**, *111*, 1657-1663, DOI: 10.1021/jp065288e

(57) Fu, H. Q.; Su, B. F.; Yang, H. Q.; Ju, C. W. Theoretical Insight into the C-H and C-C Scission Mechanism of Ethane on a Tetrahedral Pt_4 Subnanocluster. *RSC Adv.* **2015**, *5*, 40978-40989, DOI: 10.1039/c5ra06550j

(58) Hauser, A. W.; Gomes, J.; Bajdich, M.; Head-Gordon, M.; Bell, A. T. Subnanometer-sized Pt/Sn Alloy Cluster Catalysts for the Dehydrogenation of Linear Alkanes. *Phys. Chem. Chem. Phys.* **2013**, *15*, 20727-207285, DOI: 10.1039/C3CP53796J

(59) Hauser, A. W.; Horn, P. R.; Head-Gordon, M.; Bell, A. T. A Systematic Study on Pt based, Subnanometersized Alloy Cluster Catalysts for Alkane dehydrogenation: Effects of Intermetallic Interaction. *Phys. Chem. Chem. Phys.* **2016**, *18*, 10906-10917, DOI: 10.1039/c6cp00360e

(60) Yang, M. L.; Zhu, Y. A.; Zhou, X. G.; Sui, Z. J.; Chen, D. First-Principles Calculations of Propane Dehydrogenation over PtSn Catalysts. *ACS Catal.* **2012**, *2*, 1247-1258, DOI: 10.1021/cs300031d

(61) Chang, X.; Moskaleva, L.; Zhao, Z. J.; Gong, J. Activity-Selectivity Trade-off in Propane Dehydrogenation: Pt-C Repulsion is the Essence. *J. Phys. Chem. C* **2024**, *128*, 12931-12937, DOI: 10.1021/acs.jpcc.4c01253

(62) Fricke, C. H.; Bamidele, O. H.; Bello, M.; Chowdhury, J.; Terejanu, G.; Heyden, A. Modeling the Effect of Surface Platinum-Tin Alloys on Propane Dehydrogenation on Platinum−Tin Catalysts. *ACS Catal.* **2023**, *13*, 10627-10640, DOI:10.1021/acscatal.3c00939

(63) Gorczyca, A.; Raybaud, P.; Moizan, V.; Joly, Y.; Chizallet, C. Atomistic Models for Highly-Dispersed PtSn/γ-Al_2O_3 Catalysts: Ductility and Dilution Affect the Affinity for Hydrogen. *ChemCatChem* **2019**, *11*, 3941-3951, DOI: 10.1002/cctc.201900429

(64) https://nomad-lab.eu

(65) Álvarez-Moreno, M.; de Graaf, C.; Lopez, N.; Maseras, F.; Poblet, J. M.; Bo, C. Managing the Computational Chemistry Big Data Problem: The ioChem-BD Platform. *J. Chem. Inf. Model.* **2015**, *55,* 95−103, DOI: 10.1021/ci500593j.

TOC GRAPHIC